J|A|C|S
ARTICLES
Published on Web 12/08/2006

Excited-State Mixed-Valence Distortions in a Diisopropyl Diphenyl Hydrazine Cation

Jenny V. Lockard,[†] Jeffrey I. Zink,*[,†] Yun Luo,[‡] Michael N. Weaver,[‡] Asgeir E. Konradsson,[‡] Joseph W. Fowble,[‡] and Stephen F. Nelsen*[,‡]

Contribution from the Department of Chemistry and Biochemistry, University of California, Los Angeles, California 90095, and Department of Chemistry, University of Wisconsin, 1101 University Avenue, Madison, Wisconsin 53706-1396

Received February 7, 2006; E-mail: nelsen@chem.wisc.edu

Abstract: Excited-state mixed valence (ESMV) occurs in the 1,2-diphenyl-1,2-diisopropyl hydrazine radical cation, a molecule in which the ground state has a symmetrical charge distribution localized primarily on the hydrazine, but the phenyl to hydrazine charge-transfer excited state has two interchangeably equivalent phenyl groups that have different formal oxidation states. Electronic absorption and resonance Raman spectra are presented. The neighboring orbital model is employed to interpret the absorption spectrum and coupling. Resonance Raman spectroscopy is used to determine the excited-state distortions. The frequencies of the enhanced modes from the resonance Raman spectra are used together with the time-dependent theory of spectroscopy to fit the two observed absorption bands that have resolved vibronic structure. The origins of the vibronic structure and relationships with the neighboring orbital model are discussed.

Introduction

As pointed out by Ratner and Jortner,[1] photoexcitation is perhaps the most general way to couple a molecular electronics system to its environment; therefore, understanding the molecular changes that occur upon light absorption is important for considering possible applications.[2] Mixed-valence (MV) compounds are among the most basic systems that couple electron transfer with electronic excitation. The simplest type of mixed-valence system contains a symmetric bridge (B) that connects two interchangeably equivalent M groups. Many studies of M−B−M type MV molecules have focused on determining the extent of charge delocalization,[3,4] electron-transfer rates using NMR for very low electronic coupling systems,[5] ESR for dinitrogen-centered higher electronic coupling systems,[6] or IR for very rapid metal-centered systems,[7] and/or the overall reorganization energy associated with the mixed-valence transition. Fewer investigations[8−12] have focused on determining the specific structural changes that accompany the intervalence transitions perhaps because they are difficult to evaluate experimentally. Mixed-valence absorption bands often lack vibronic structure that indicates the excited-state geometry changes accompanying the charge transfer. Resonance Raman spectroscopy provides information on excited-state geometry changes by indicating which vibrational modes are most important in the mixed-valence transition. However, mixed-valence bands often occur at relatively low energy (>1000 nm) which is out of the range of most laser lines traditionally used for resonance Raman spectroscopy.

A new addition to the field, excited-state mixed valence (ESMV), provides information unavailable from its ground-state analogue (such as the sign of the coupling and readily measurable details about the reorganization energies). ESMV occurs in molecules in which the ground state has a symmetrical charge distribution but the excited-state possesses two or more interchangeably equivalent sites that have different formal oxidation states. The ESMV absorption band results from the transition from the ground state to a coupled excited-state where two equivalent charge distributions are possible. There are two

[†] University of California.
[‡] University of Wisconsin.

(1) Ratner, M. A.; Jortner, J. *Molecular Electronics*; Jortner, J., Ratner, M., Eds.; Blackwell Science: London, 1997; p 5.
(2) de Silva, A. P., Ed. *Molecular-Level Electronics*; Balzani, V., Ed.; Electron Transfer in Chemistry, Vol. V, Part 1; Wiley-VCH: Weinheim , 2001; p 1.
(3) Creutz, C. *Prog. Inorg. Chem.* **1983**, *30*, 1.
(4) Crutchley, R. J. *Adv. Inorg. Chem.* **1994**, *41*, 273.
(5) Elliott, C. M.; Derr, D. L.; Matyushov, D. V.; Newton, M. D. *J. Am. Chem. Soc.* **1998**, *120*, 11714.
(6) (a) Nelsen, S. F.; Ismagilov, R. F.; Powell, D. R. *J. Am. Chem. Soc.* **1997**, *119*, 10213. (b) Nelsen, S. F.; Ismagilov, R. F.; Gentile, K. E.; Powell, D. R. *J. Am. Chem. Soc.* **1999**, *121*, 7108. (c) Nelsen, S. F.; Konradsson, A. E.; Teki, Y. *J. Am. Chem. Soc.* **2006**, *128*, 2902.
(7) Demadis, K. D.; Hartshorn, C. M. Meyer, T. J. *Chem. Rev.* **2001**, *101*, 2655.
(8) Bailey, S. E.; Zink, J. I.; Nelsen, S. F. *J. Am. Chem. Soc.* **2003**, *125*, 5939.
(9) Rocha, R. C.; Brown, M. G.; Londergan, C. H.; Salsman, J. C.; Kubiak, C. P.; Shreve, A. P. *J. Phys. Chem. A* **2005**, *109*, 9006.
(10) Londergan, C. H.; Rocha, R. C.; Brown, M. G.; Shreve, A. P.; Kubiak, C. P. *J. Am. Chem. Soc.* **2003**, *125*, 13912.
(11) Williams, R. D.; Hupp, J. T.; Ramm, M. T.; Nelsen, S. F. *J. Phys. Chem. A* **1999**, *103*, 11172.
(12) Gamelin, D. R.; Bominaar, E. L.; Mathoniere, C.; Kirk, M. L.; Wieghardt, K.; Girerd, J.-J.; Solomon, E. I. *Inorg. Chem.* **1996**, *35*, 4323.

10.1021/ja0609093 CCC: $33.50

transition dipole moments that have parallel and/or antiparallel components. A Marcus−Hush-type two-state diagram can represent the lowest excited state. The corresponding absorption band splits into two components when the coupling is large enough. The adiabatic energy surfaces for the ESMV system can either have two localized energy minima that are displaced from that of the ground state (a Robin-Day "Type II" excited-state diagram), or the ground- and both excited-state surfaces can have minima at the same configuration coordinate (a "Type III" diagram) when the coupling is large. The angle between the transition dipoles can be obtained from the relative absorbances of the components of the transitions. In contrast to ground state MV, the sign of the electronic coupling becomes important for ESMV and can be determined from the absorbances.

Several examples of excited-state mixed valence have been studied.[13,14] Recently, we have studied the 2,3-diphenyl-2,3-diazabicyclo[2.2.2]octane cation, $\mathbf{2}^+$ which has a mixed-valence excited-state produced by the phenyl to hydrazine electronic transition.[14] The +1 charge is symmetrically located and principally on the hydrazine bridge in the ground state. Upon excitation, charge is transferred to the phenyl groups, and formally, either phenyl group could donate an electron to the $(NN)^+$ unit. The excited-state can be modeled as two interacting diabatic surfaces which couple as a result of the through-bond orbital mixing of the phenyl groups with the bridging hydrazine unit. Since ESMV transitions usually occur at higher energy than those of ground-state MV systems, detailed vibrational studies by resonance Raman spectroscopy are more experimentally feasible. Resonance Raman studies of $\mathbf{2}^+$ indicate that the most highly distorted symmetric modes involve CNNC twisting motion in the low-frequency region and C−N and N−N distortions in the higher-frequency region. The displacements along these symmetric coordinates were used to explain the bandwidth of the ESMV band.

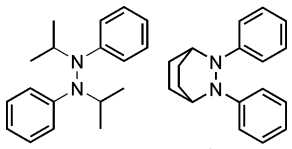

1 **2**

In this paper, the related compound, 1,2-diphenyl-1,2-diisopropyl hydrazine radical cation, $\mathbf{1}^+$, is investigated. Although $\mathbf{1}^+$ and $\mathbf{2}^+$ have structural similarities, their absorption spectra are significantly different, and $\mathbf{1}^+$ is the first hydrazine radical cation out of many that have been examined[15−17] that shows vibronic fine structure in its absorption spectrum (see Results). This vibronic structure in conjunction with the resonance Raman studies yields the most complete analysis of the structural changes that are associated with an ESMV system to date. The assignments of the low-energy excited states and the analysis and interpretation of the distortions causing the vibronic structure are discussed. The neighboring orbital model[14,18−32] is used to determine the sign of the coupling. This model focuses on the symmetry-based mixing of the molecular orbitals of the hydrazine bridge and the phenyl groups. The absorption bands of $\mathbf{1}^+$ are assigned with the use of this model. The experimental absorption spectrum is fit by using the time-dependent theory of spectroscopy.[33−53] The vibrational mode frequencies and distortions used in the calculation are obtained from the resonance Raman spectra. The different vibrational structure of the high- versus low-energy absorption band is discussed.

Experimental Section

1. Synthesis. *N,N′*-Diisopropyl-*N,N′*-diphenyl Hydrazine (1). A modification of the method of Reesor and Wright[54] was employed. A mixture of 1.5 g of sodium and 1.3 g of azobenzene was stirred in 50 mL of freshly distilled THF under nitrogen for 24 h. Isopropylmethanesulfonate (4 mL) was added and the mixture stirred an additional 24 h. After removal of excess sodium, aq sodium hydroxide and ether were added, the organic layer was separated, and the aqueous layer was extracted with ether. After removal of solvent under reduced pressure from the combined organic layers, the residue was crystallized from methanol, giving 0.9 g of **1** (41%), mp 92−93 °C (lit.[54] 93−93.5).

The radical cation $\mathbf{1}^+$ was made by oxidation of **1** in dry acetonitrile or butyronitrile using nitrosyl tetrafluoroborate (for Raman spectroscopy) or tris(*p*-bromophenyl)aminium hexachlorophosphate (for optical spectroscopy).

***N,N′*-Diethyl-*N,N′*-diphenyl Hydrazine (4)** was also made by the method of Reesor and Wright.[54]

2. Absorption and Resonance Raman Spectroscopy. The absorption spectrum of $\mathbf{1}^+$ in acetonitrile was obtained using a Cary 5000

(13) (a) Lockard, J. V.; Zink, J. I.; Konradsson, A. E.; Weaver, M. N.; Nelsen, S. F. *J. Am. Chem. Soc.* **2003**, *125*, 13471. (b) Lockard, J. V.; Zink, J. I.; Trieber, D. A.; Konradsson, A. E.; Weaver, M. N.; Nelsen, S. F. *J. Phys. Chem. A* **2005**, *109*, 1205.
(14) Plummer, E. A.; Zink, J. I. *Inorg. Chem.* **2006**, *45*, 6556.
(15) Nelsen, S. F.; Blackstock, S. C.; Yumibe, N. P.; Frigo, T. B.; Carpenter, J. E.; Weinhold, F. *J. Am. Chem. Soc.* **1985**, *107*, 143.
(16) Nelsen, S. F.; Frigo, T. B.; Kim, Y.; Blackstock, S. B. *J. Am. Chem. Soc.* **1989**, *111*, 5387.
(17) Nelsen, S. F.; Tran, H. Q.; Ismagilov, R. F.; Chen, L.-J; Powell, D. R. *J. Org. Chem.* **1998**, *63*, 2536.
(18) Nelsen, S. F.; Weaver, M. N.; Luo, Y.; Lockard, J. V.; Zink, J. I. *Chem. Phys.* **2006**, *324*, 195.
(19) Hoffmann, R. *Acc. Chem. Res.* **1971**, *4*, 1.
(20) Verhoeven, J. W.; Pasman, P. *Tetrahedron* **1981**, *37*, 943.
(21) Paddon-Row, M. N.; Shephard, M. J. *J. Am. Chem. Soc.* **1997**, *119*, 5355.
(22) Whangbo, M. H.; Hoffman, R. *J. Chem. Phys.* **1978**, *68*, 5498.
(23) Marsman, A. W.; Havenith, R. W. A;, Bethke, S.; Jenneskens, L. W.; Gleiter, R.; van Lenthe, J. H. *Eur. J. Org. Chem.* **2000**, *14*, 2629.
(24) Heilbronner, E.; Schmelzer, A. *Helv. Chim. Acta* **1975**, *58*, 936.
(25) Dougherty, D.; Brint, P.; McGlynn, S. P. *J. Am. Chem. Soc.* **1978**, *100*, 5597.
(26) Gleiter, R.; Lange, H.; Borzyk, O. *J. Am. Chem. Soc.* **1996**, *118*, 4889.
(27) Newton, M. D. *Chem. Rev.* **1991**, *91*, 767.
(28) Paddon-Row, M. N. *Acc. Chem. Res.* **1982**, *15*, 245.
(29) Gleiter, R.; Schaifer, W. *Acc. Chem. Res.* **1990**, *23*, 369.
(30) De, Ridder, D.; Goubitz, K.; Shenk, H.; Krijnen, B.; Verhoeven, J. W. *Helv. Chim. Acta* **2003**, *86*, 799.
(31) Sarneel, R.; Worrell, C. W.; Pasman, P.; Verhoeven, J. W.; Mes, G. F. *Tetrahedron* **1980**, *36*, 3241.
(32) Imamura, A.; Ohsaku, M. *Tetrahedron* **1981**, *37*, 2191.
(33) Lee, S.-Y.; Heller, E. J. *J. Chem. Phys.* **1979**, *71*, 4777.
(34) Heller, E. J. *Acc. Chem. Res.* **1981**, *14*, 368.
(35) Heller, E. J.; Sundberg, R. L.; Tannor, D. *J. Phys. Chem.* **1982**, *86*, 1822.
(36) Zink, J. I.; Shin, K.-S. K. In *Advances in Photochemistry*; Wiley: New York, 1991; Vol. 16, p 119.
(37) Reber, C.; Zink, J. I. *J. Chem. Phys.* **1992**, *96*, 2681
(38) Shin, K.-S. K.; Zink, J. I. *Inorg. Chem.* **1989**, *28*, 4358.
(39) Acosta, A.; Zink, J. I. *J. Organomet. Chem.* **1998**, *554*, 87.
(40) Reber, C.; Zink, J. I. *Comments Inorg. Chem.* **1992**, *13*, 177.
(41) Wexler, D.; Zink, J. I.; Reber, C. In *Electronic and Vibronic Spectra of Transition Metal Complexes I*; Yersin, H., Ed.; Springer-Verlag: Berlin, Heidelberg, 1994; p 174.
(42) Shin, K. S.; Clark, R. J. H.; Zink, J. I. *J. Am. Chem. Soc.* **1990**, *112*, 3754.
(43) Shin, K. S.; Clark, R. J. H.; Zink, J. I. *J. Am. Chem. Soc.* **1990**, *112*, 7148.
(44) Zink, J. I. *Coord. Chem. Rev.* **2001**, *211*, 69.
(45) Myers, A. B. In *Laser Techniques in Chemistry*; Wiley: New York, 1995; Vol. 23, p 325.
(46) Kelly, A. M. *J. Phys. Chem. A* **1999**, *103*, 6891.
(47) Myers, A. B. *Chem. Rev.* **1996**, *96*, 911.
(48) Myers, A. B. *Acc. Chem. Res.* **1997**, *30*, 519.
(49) Hanna, S. D.; Zink, J. I. *Inorg. Chem.* **1996**, *35*, 297
(50) Wootton, J. L.; Zink, J. I. *J. Phys. Chem.* **1995**, *99*, 7251.
(51) Henary, M.; Wootton, J. L.; Khan, S. I.; Zink, J. I. *Inorg. Chem.* **1997**, *36*, 796.
(52) Henary, M.; Zink, J. I. *J. Am. Chem. Soc.* **1989**, *111*, 7407.
(53) Shin, K. S. K.; Zink, J. I. *J. Am. Chem. Soc.* **1990**, *112*, 7148.
(54) Reesor, J. W. B.; Wright, G. F. *J. Org. Chem.* **1957**, *22*, 375.

UV−vis−nIR spectrophotometer. Raman spectra were obtained using a triple monochromator equipped with a Princeton Instruments LN-CCD. Data were processed by a PC computer. The 676 and 413 nm lines of a Coherent I-300 Krypton laser and the 514, 488, and 457 nm lines of a Coherent Argon laser at ~100 mW were used for excitation. The spectra were collected from an acetonitrile solution sample of $\mathbf{1}^+$.

Theoretical and Numerical Methods

Electronic spectra for excited-state mixed-valence potential surfaces are calculated in the framework of the time-dependent theory of molecular spectroscopy.[33−37] The theoretical foundation underlying these calculations has been described previously. In this section, the theory underlying the calculation of absorption spectra is briefly presented.

The fundamental equation for the calculation of an absorption spectrum in the time dependent theory is:

$$I(\omega) = C\omega \int_{-\infty}^{+\infty} \exp(i\omega t)\left\{\langle\Phi|\Phi(t)\rangle \exp\left(-\Gamma^2 t^2 + \frac{iE_0}{h}t\right)\right\}\mathrm{d}t \quad (1)$$

with $I(\omega)$ the absorbance at frequency ω, E_o the energy of the electronic origin transition, and Γ a phenomenological Gaussian damping factor.[38] The most important part of eq 1 is $\langle\Phi|\Phi(t)\rangle$, the autocorrelation function of the wavepacket Φ prepared on an excited-state potential surface after the spectroscopic transition, with the wavepacket $\Phi(t)$ developing on this surface with time. In the absence of coupling terms between the normal coordinates, the total autocorrelation in a system with K coordinates is given by:

$$\langle\Phi|\Phi(t)\rangle = \prod_k \langle\phi^k|\phi^k(t)\rangle \quad (2)$$

where ϕ^k is a wavepacket associated with coordinate k ($k = 1, ..., K$).

For simplicity we chose harmonic potentials in all of the following examples, although the methods used are not restricted by the functional form of the potentials. The displacement of the minimum of one electronic state from the other, from that of the ground state, ΔQ, is abbreviated as Δ in this paper. The potentials are given by:

$$V_j(Q) = \frac{1}{2}k_j(Q \pm \Delta Q_j)^2 + E_j \quad (3)$$

with $k_j = 4\pi^2 M(h\omega_j)^2$ the force constant, ΔQ_j the positions of the potential minima along Q, and E_j the energy of the potential minimum for state j.

The lowest-energy conformations for dihpenyldiisopropyl hydrazine were optimized using Spartan '02,[55] and the Gaussian 98 program suite was used for frequency calculations.[56] The Koopmans-based calculations required two-single point calculations in Gaussian 98, those of the neutral in cation geometry and of the dication in cation geometry. The intensities for the Koopmans-based calculations were determined using NBO 5.0[57] and the DIMO keyword. All calculations employed the Standard Pople style 6-31G* basis set as implemented in Spartan and Gaussian and the B3LYP[58] density functional was applied in each case. Geometry optimizations were performed using standard gradient methods. Calculated vibrational modes were viewed using MOLDEN[59] and GaussView 2.0.

(55) Spartan'02, Wavefunction, Inc., Irvine CA.
(56) M. J. Frisch; et al. *Gaussian 98*, Ver. A.9; Gaussian, Inc.: Pittsburgh PA, 1998.
(57) NBO 5.0. Glendening, E. D.; Badenhoop, J. K.; Reed, A. E.; Carpenter, J. E.; Bohmann, J. A.; Morales, C. M.; Weinhold, F. Theoretical Chemistry Institute, University of Wisconsin: Madison, WI, 2001.
(58) (a) Becke, A. D. *J. Chem. Phys.* **1993**, *98*, 5648. (b) Becke, A. D. *Phys. Rev. A* **1988**, *38*, 3098. (c) Lee, C.; Yang, W.; Parr, R. G. *Phys. Rev. B* **1988**, *37*, 785. (d) Vosko, S. H.; Wilk, S. H.; Nusair, M. *Can. J. Phys.* **1980**, *58*, 1200.
(59) Schaftenaar, G.; Noordik, J.H. Molden: a pre- and post-processing program for molecular and electronic structures. *J. Comput.-Aided Mol. Des.* **2000**, *14*, 123.

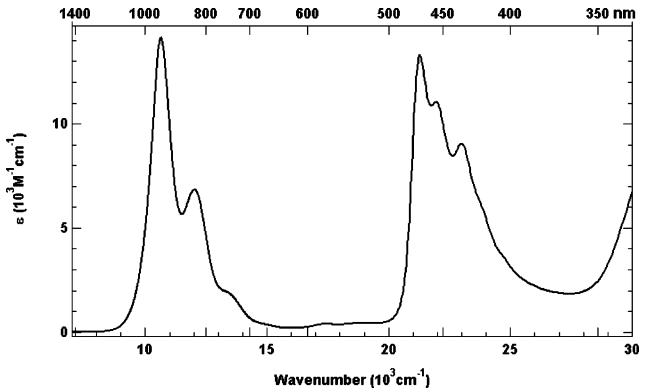

Figure 1. Absorption spectrum for $\mathbf{PhiPrN)_2}^+$ in acetonitrile, oxidant $(BrC_6H_4)_3N^{\bullet+}SbCl_6^-$.

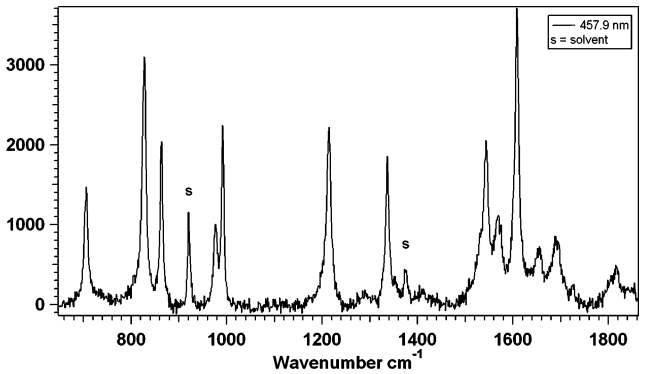

Figure 2. Resonance Raman spectra of $\mathbf{1}^+$ obtained using 458-nm excitation. The letter "s" indicates acetonitrile solvent peaks.

Results

1. Absorption Spectra. The room-temperature absorption spectrum of $\mathbf{1}^+$ in acetonitrile solution is shown in Figure 1.

The lowest-energy band has a peak maximum at 10650 cm^{-1} and an extinction coefficient of 14 100 M^{-1} cm^{-1}. A vibronic progression is observed for this band with 1395 cm^{-1} peak spacings. The next-higher energy intense band has a peak maximum at 21 280 cm^{-1} and an extinction coefficient of 13 300 M^{-1} cm^{-1}. It also has vibronic structure with resolved vibronic peaks separated by ~700 and ~1700 cm^{-1} from the E_{oo} band. Two low-intensity peaks are observed at 17400 and 18900 cm^{-1} ($\epsilon < 450$ M^{-1} cm^{-1}). Some of the intensity in this region may result from an impurity or side product of the oxidation reaction because the intensity of those bands relative to that of the other bands varies over time and from one sample of oxidized product to another. The spectrum in Figure 1 represents the purest sample because it has the lowest intensity in this region.

2. Resonance Raman spectra. Resonance Raman spectra were obtained using 676 nm excitation, which is in resonance with the high-energy tail of the lower-energy absorption band, and 476, 472, 465, and 458 nm excitations, which are all in resonance with the higher-energy band at 21 280 cm^{-1} (470 nm). The resonance Raman spectrum obtained with 458 nm excitation is shown in Figure 2, and the Raman frequencies and intensities (relative to the acetonitrile solvent band at 918 cm^{-1}) of the spectra obtained with 676 and 458 nm excitation are presented in Table 1.

Discussion

1. Excited-State Mixed Valence. The excited-state mixed-valence behavior of **1** is modeled by two interacting harmonic

Table 1. Resonance Raman Frequencies, ω, and Intensities, I, Normalized to the Intensity of the 918 cm^{-1} Acetonitrile Band, I', Obtained Using 458 and 676 nm Excitation

$I/I'_{458\ nm}$	$\Delta_{458\ nm}$[a]	$\Delta_{458\ nm}$ for fit[b]	$I/I'_{676\ nm}$	$\Delta_{676\ nm}$[a]	$\Delta_{676\ nm}$ for fit[b]	ω, cm^{-1}	calc ω cm^{-1}	assignment
2.68	0.6	1.05				705	704	Ph ring def. + sp^2/sp^3 twist
5.27	0.74	0.45	0.02	0.36	0.36	827	778	sp^2/sp^3 twist w/ Ph CH wag
2.56	0.48	0.3	0.01	0.26	0.26	864	847	Planar Ph. twist w/ CH wag
1.39	0.31	0.2				977	982	Ph CH wag w/ sm. ring def.
2.14	0.38	0.3				991	992	NN rock w/ Ph ring breathing
4.58	0.45	0.4	0.1	0.51	0.51	1215	1216	NN str. w/ Ph. CH in plane wag
3	0.33	0.20	0.09	0.43	0.43	1336	1304	NN str. + CN str.
5.14	0.38	0.3				1543	1526	Ph CN w/ CH wag
2.88	0.28	0.1				1570	1530	Ph CN w/ CH wag
7	0.42	0.15	0.24	0.59	0.59	1607	1631	Ph CC str.
			0.04	0.24	0.24	1635		
2.23	0.23	0.05				1655	1640	Ph CC str.
2.88	0.26	0.07				1688		
2.14	0.21	0.74				1816		

[a] Displacement, Δ obtained using Savin's formula.[36] [b] Actual displacement used for calculated fit of absorption spectrum.

potential energy surfaces in the excited-state as shown in Figure 3. A single harmonic surface (*gs*) with its minimum at zero along the normal vibrational coordinate represents the ground state with the charge localized on the nitrogens. Two possible electronic transitions from the phenyl group to the hydrazine unit send the +1 charge to one phenyl group or the other. Symmetry requires that these transitions be equal in energy and occur with equal probability. In the model, these energetically equal transitions give rise to two diabatic surfaces in the excited-state that are degenerate at $Q = 0$, each representing the system with the charge localized on one phenyl. The excited-state diabatics are displaced from the ground-state surface such that the Frank-Condon region of each diabatic has a nonzero slope that is equal in magnitude and opposite in sign. The diabatic surfaces couple, creating two new nondegenerate adiabatic surfaces (shown as the solid *u*pper and *l*ower excited-state wells) with an energy splitting of $\Delta E^{ex} = 2H_{ab}^{ex}$ at $Q = 0$ between the lower- and the higher-energy adiabatic surfaces. The degree of charge delocalization in the excited state is dictated by the ratio of ΔE^{ex} to λ^{ex}. In Figure 3, ΔE^{ex} is sufficiently large to produce a single minimum in the lower adiabatic, that is $H_{ab}^{ex} > \lambda^{ex}/2$. The surfaces are depicted along an asymmetric normal coordinate.

The absorption spectrum of $\mathbf{1}^+$, as shown in Figure 1, reveals the effects of coupling along this asymmetric coordinate in the excited state. The two absorption band components at 10 650 cm^{-1} and 17 400 cm^{-1} correspond to the transition to the lower and upper adiabatic surfaces, respectively. The difference in energy between these two peak maxima is equal to twice the excited-state coupling; therefore, H_{ab}^{ex} is about 3500 cm^{-1} according to the three-state ESMV model. If the coupling had been zero, a single peak would have been observed in the absorption spectrum because the transition to one diabatic surface produces the same spectrum as a transition to the other. The difference in the absorptivities of the two components is a result of the antiparallel transition dipole moments that are discussed next.

2. Transition Dipole Moments. The transition dipole moments for transitions to the two diabatic states are equal in magnitude by symmetry. They are opposite in sign if the transition to the bridging group occurs from symmetry equivalent groups on opposite sides of the bridge as is the case for **1**. The transition dipole moments are antiparallel. (If the donating groups were on the same side of the bridge as is the case for **2**, the dipoles have vector components in the same direction and have the same sign.) The transition dipole moment matrix in the diabatic basis that represents the transition from the ground state to the two diabatic states is

$$\mu_d = \begin{pmatrix} 0 & \pm\mu_1 & \mu_2 \\ \pm\mu_1 & 0 & 0 \\ \mu_2 & 0 & 0 \end{pmatrix} \tag{4}$$

The negative signs apply for antiparallel transitions and positive signs apply for parallel transitions. The transformation to the adiabatic basis gives

$$\mu_a = \begin{pmatrix} 0 & \pm\mu_1 \cos\vartheta + \mu_2 \sin\vartheta & \mp\mu_1 \sin\vartheta + \mu_2 \cos\vartheta \\ \pm\mu_1 \cos\vartheta + \mu_2 \sin\vartheta & 0 & 0 \\ \mp\mu_1 \sin\vartheta + \mu_2 \cos\vartheta & 0 & 0 \end{pmatrix} \tag{5}$$

where

$$\tan 2\vartheta = \frac{2H_{ab}^{ex}}{V_1(Q) - V_2(Q)} \tag{6}$$

Diabatic-to-adiabatic basis transformations of transition dipole moments for ground-state mixed valence have been presented in the literature.[60−62]

(60) Cave, R. J.; Newton, M. D. *J. Chem. Phys.* **1997**, *106*, 9213.

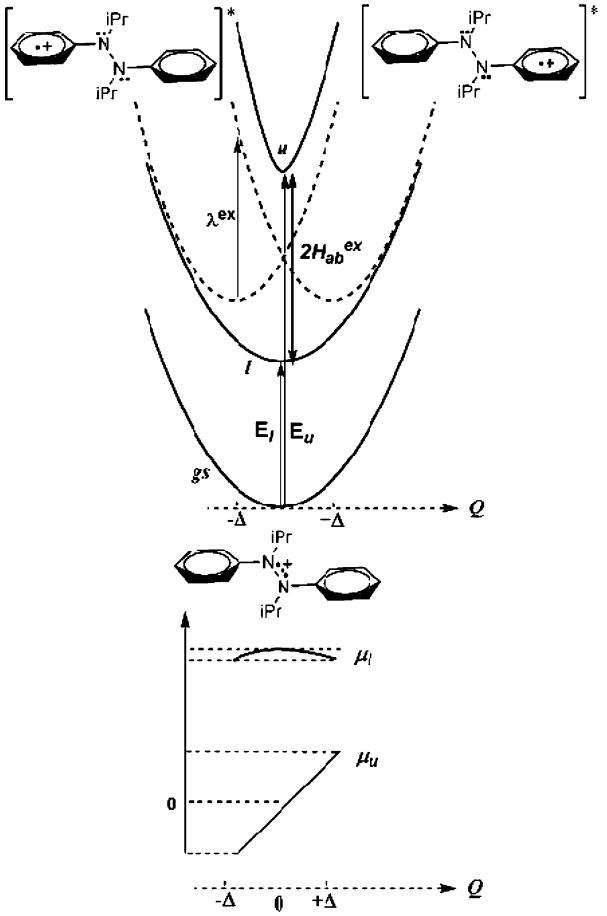

Figure 3. Potential energy surfaces as a function of an asymmetric coordinate. The lowest-energy surface represents the ground electronic state. The pair of surfaces at higher-energy represents the mixed-valence excited electronic state. The solid lines are the adiabatic surfaces; the dotted lines are diabatic surfaces. The transition dipole moments for the adiabatic surfaces are plotted as a function of the vibrational coordinate below the surfaces. That for the lower adiabatic surface, μ_l, is always nonzero, but that for the upper adiabatic surface, μ_u, changes sign at the origin.

The adiabatic state represented by the wavefunction, $\Psi^+ = \cos\theta\,\Psi_1 + \sin\theta\,\Psi_2$ is the in-phase combination of the diabatic functions and that represented by the wavefunction $\Psi^- = -\sin\theta\,\Psi_1 + \cos\theta\,\Psi_2$ is the out-of-phase combination. The relative energies of these two states are determined by the sign of H_{ab}^{ex} which is discussed in detail in the next section. In the adiabatic basis the transition dipole to the surface represented by Ψ^+ is $\mu_u = \mp\mu_1 \sin\vartheta + \mu_2 \cos\vartheta$. For antiparallel transition dipole moments the negative sign applies and this function is zero at $Q = 0$ but is positive when $Q > 0$ and negative when $Q < 0$. The physical meaning is that the transition is electric dipole forbidden at the internuclear equilibrium geometry but is vibronically allowed. In contrast, the transition dipole to the state represented by Ψ^- is $\mu_l = \pm\mu_1 \cos\vartheta + \mu_2 \sin\vartheta$. The positive sign applies for anti-parallel dipole moments, and this function is nonzero everywhere along the Q coordinate. In the case of parallel transition dipole moments, the signs are reversed; the transition to the surface represented by Ψ^- is dipole forbidden and that to the surface represented by Ψ^+ is dipole allowed.

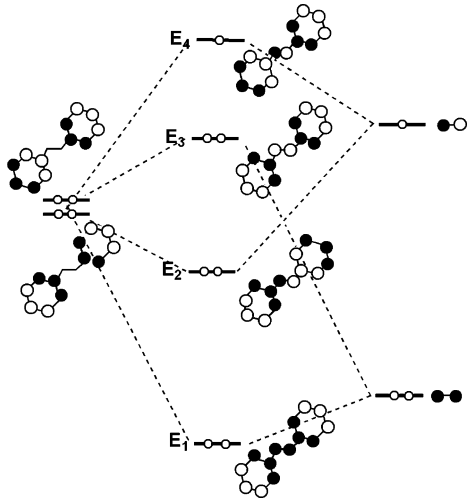

Figure 4. Neighboring orbital analysis applied to $\mathbf{1}^+$. Degenerate diabatic antisymmetric and symmetric phenyl orbital combination pairs (shown on the left) mix with the half-filled diabatic antisymmetric and filled symmetric NN π orbitals to produce the pattern of adiabatic combination orbitals shown. The isopropyl groups have been omitted for clarity. The $E_3 \rightarrow E_4$ transition corresponds to E_l in Figure 3, and $E_2 \rightarrow E_4$ corresponds to E_u. The energy difference is $2H_{ab}^{ex}$.

3. Neighboring Orbital Analysis of $\mathbf{1}^+$ and Absorption Band Assignment. The sign of the coupling has a profound influence on excited-state mixed-valence spectroscopy because it determines the identities of the lowest- and highest-energy adiabatic states. For through-space coupling, the sign is intrinsically negative. The reason is reminiscent of simple molecular orbital theory where the in−phase overlap between two orbitals produces a bonding molecular orbital (no nodes), and the exchange integral β is thus defined as negative. However, when the coupling is mediated by other orbitals in a molecule, the sign can be positive.

The neighboring orbital model can be used to interpret the through-bond coupling in $\mathbf{1}^+$.[14,18−32] A simple physical representation of the model applied to this system is shown in Figure 4.

The bridge orbitals of interest are the NN π bonding and π antibonding orbitals. The NN π bonding orbital has the appropriate symmetry to mix with the in-phase combination, $\pi_{Ph} + \pi_{Ph}$ and the NN π antibonding orbital has the appropriate symmetry to mix with the out-of-phase combination, $\pi_{Ph} - \pi_{Ph}$. When the orbitals of the same symmetry mix, the degeneracy of the linear combinations, $\pi_{Ph} + \pi_{Ph}$ and $\pi_{Ph} - \pi_{Ph}$ is removed. As illustrated by the molecular orbitals at the center of Figure 4, the energy of the molecular orbital containing the $\pi_{Ph} + \pi_{Ph}$ combination is higher than that containing the $\pi_{Ph} - \pi_{Ph}$ combination. This is the opposite order from that expected if the usual negative through-space coupling were operative. Therefore, the coupling is positive.

There are seven electrons in the neighboring orbitals of $\mathbf{1}^+$; both aryl orbitals are occupied, and the odd electron is in the N−N π^* orbital in the ground electronic state. The two mixed-valence excited states result from the promotion of an electron from one of the two degenerate aryl orbitals to the N−N π^* orbital. The orbitals at the center of Figure 4, labeled E_1 through E_4, represent the adiabatic limit. The ground-state electron configuration in this basis is $(E_1)^2(E_2)^2(E_3)^2(E_4)^1$ and the two mixed-valence excited-state electron configurations are

(61) Newton, M. D.; Cave, R. J. *Molecular Electronics*; Jortner, J., Ratner, M., Eds.; Blackwell Science: Oxford, 1997; p 73.
(62) Cave, R. J.; Newton, M. D. *Chem. Phys. Lett.* **1996**, *249*, 15.

$(E_1)^2(E_2)^2(E_3)^1(E_4)^2$ and $(E_1)^2(E_2)^1(E_3)^2(E_4)^2$. The latter two states are represented by the lower and upper adiabatic surfaces respectively in Figure 3. Note that the state arising from the E_1 to E_4 transition, $(E_1)^1(E_2)^2(E_3)^2(E_4)^1$, is not represented in Figure 3. A detailed description of the electronic states corresponding to the neighboring orbital model can be found in ref 18. For antiparallel transition dipole moments, as is the case for $\mathbf{1}^+$, the transition to the orbital containing the out-of-phase combination, $\pi_{Ph} - \pi_{Ph}$ (E_3) is fully allowed, while the transition to the orbital containing the in-phase combination, $\pi_{Ph} + \pi_{Ph}$ (E_2), is dipole forbidden. The lowest-energy room-temperature absorption band at 10 650 cm^{-1} is therefore assigned to the electronic transition from the E_3 to the E_4 orbital, giving rise to the first neighboring orbital excited state, $(E_1)^2(E_2)^2(E_3)^1(E_4)^2$. The next-higher energy intense band at 21 280 cm^{-1} is assigned to the transition from the E_1 to E_4 orbital, which results in the highest-energy state in the neighboring orbital system, $(E_1)^1(E_2)^2(E_3)^2(E_4)^2$. Because the $E_2 \rightarrow E_4$ transition is electric dipole forbidden, the weak absorption band between the bands assigned to the $E_3 \rightarrow E_4$ and $E_1 \rightarrow E_4$ transitions may be attributed to the vibronically allowed $E_2 \rightarrow E_4$ transition. While some of the intensity of the weak bands at 17 200 and 18 800 cm^{-1} may arise from a side product of the oxidation reaction, the majority of the intensity may be attributed to the vibronically allowed $E_2 \rightarrow E_4$ transition.

The energy gap between the highest occupied molecular orbital (*homo*) and *homo*-1 orbitals of neutral tetraalkylhydrazines that are calculated at the geometry of the radical cations using semiempirical methods has been shown to correlate surprisingly well with the large changes in the transition energies in the optical spectra of the radical cations.[15−17] This demonstrates that Koopmans theorem[63] works well even when large changes in geometry between the ground and excited states occur. More recently, we have shown that Koopmans-based calculations, those on radical ions that have the singly occupied molecular orbital (*somo*) either (a) filled by adding an electron, as done previously, or (b) emptied by removing one provide estimations of the effective energy gaps between the filled orbitals and the *somo* (using (a)) and between the *somo* and the virtual orbitals (using (b)) that are useful in interpreting the optical spectra of a wide variety of radical ions.[64−66] Figure 5 shows the results of a neutral in cation geometry calculation at the (U)B3LYP/6-31G* level on $\mathbf{3}^+$, the dimethyl analogue of $\mathbf{1}^+$. The orbitals are labeled with their neighboring orbital designations (see Figure 4). It should be noted that the lowest calculated transition energies, (E_4-E_3, 11 000 cm^{-1}) is close to the observed first transition for $\mathbf{1}^+$, 350 cm^{-1} higher. Two intervening orbitals that are not part of the neighboring orbital system because they have nodes through the CN bonds and do not mix, are shown to the left of the energy levels in Figure 5.

One reason for showing the calculation for $\mathbf{3}^+$ instead of the compound studied, $\mathbf{1}^+$, is its conformational simplicity. $\mathbf{3}^+$ has a single energy minimum, while $\mathbf{1}^+$ is conformationally complex because it has several minima corresponding to various isopropyl group rotations, and these affect the calculated spectrum strongly

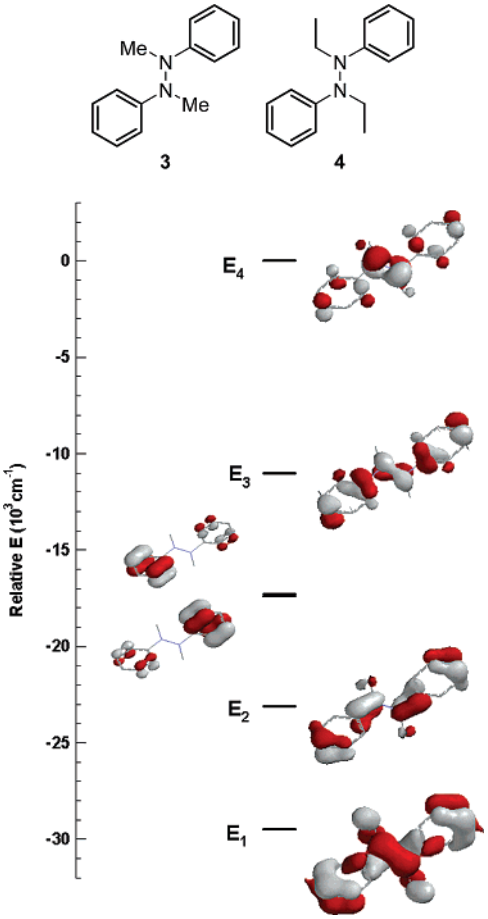

Figure 5. Koopmans-based calculation on $\mathbf{3}^+$ ($\mathbf{PhMeN})_2^+$).

because they affect the phenyl, N lone pair twist angles (ϕ_{CN}). $\mathbf{3}^+$ proved to be too unstable for us to record its optical spectrum experimentally, but the ethyl-substituted compound $\mathbf{4}^+$ was studied, although it is significantly less stable than $\mathbf{1}^+$. $\mathbf{4}^+$ has an optical spectrum that is very similar to that of $\mathbf{1}^+$. $\mathbf{4}^+$ shows bands at 10 670 and 21 370 cm^{-1} having similar vibronic structure to $\mathbf{1}^+$ in each. These similarities suggest to us that their conformations are similar, including ϕ_{CN}. UB3LYP/6-31G* calculations predict a 2890 cm^{-1} shift to higher energy for the minimum energy conformation of $\mathbf{1}^+$ compared to that of $\mathbf{4}^+$, which is certainly not observed experimentally, suggesting to us that the proper isopropyl group rotamer and hence ϕ_{CN} angle has not been obtained correctly by these calculations. Details of the calculations will not be discussed here because it has not yet been possible to address the isopropyl group conformation of $\mathbf{1}^+$ at room temperature and a meaningful comparison with experiment cannot be made.

4. Vibrational Mode Assignments. The vibronic structure of the two absorption bands shown in Figure 1 is caused by displacements of the excited-state surfaces along the symmetric coordinates. Resonance Raman spectroscopy is used to determine the frequencies of the most important symmetric modes. Vibrational assignments are made by comparing the calculated vibrational mode frequencies with the observed resonance Raman frequencies as presented in Table 1. The mode at 705 cm^{-1} involves significant C−N−N−C twist angle change and those between 800 and 1000 cm^{-1} involve phenyl ring deformation and rocking. The modes at 1215 and 1336 cm^{-1} are assigned to symmetric modes with significant N−N stretching

(63) Koopmans, T. *Physica* **1934**, *1*, 104.
(64) Nelsen, S. F.; Konradsson, A. E.; Telo. J. P. *J. Am. Chem. Soc* **2005**, *127*, 920.
(65) Nelsen, S. F.; Weaver, M. N.; Telo, J. P.; Zink, J. I. *J. Am. Chem. Soc.* **2005**, *127*, 10611.
(66) Nelsen, S. F.; Weaver, M. N.; Telo, J. P.; Lucht, B. L.; Barlow, S. *J. Org. Chem.* **2005**, *70*, 9326.

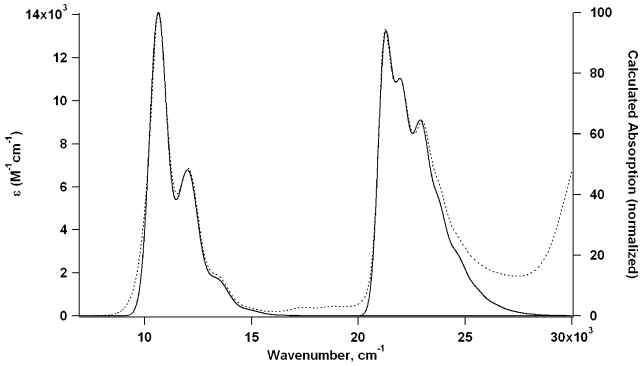

Figure 6. Calculated (solid line) and observed (dotted) room temperature absorption spectra of $\mathbf{1}^+$.

character and the modes at 1543 and 1570 cm^{-1} are assigned to symmetric C−N stretching modes. The modes above 1600 cm^{-1} involve phenyl ring CC stretching.

5. Calculated Fit of the Absorption Bands. In this section, the calculated fits to the experimental absorption bands of $\mathbf{1}^+$ are presented. As discussed in sections 2 and 3, only the $E_3 \rightarrow E_4$ excited-state mixed-valence transition is electric dipole allowed. The intensity in the 18 000 cm^{-1} region is assigned to the $E_2 \rightarrow E_4$ transition because it is vibronically allowed. On the basis of the energy separation between the lowest energy $E_3 \rightarrow E_4$ band and the next higher energy feature at 17 400 cm^{-1}, the effective coupling (i.e., half the energy separation between E_2 and E_3) is approximately 3500 cm^{-1}. This magnitude of coupling is similar to that of $\mathbf{2}^+$ which was determined to be 3 750 cm^{-1}. Because this system is highly delocalized, the adiabatic surfaces along the asymmetric electron-transfer coordinate possess single minima which are undisplaced from the ground-state surface. For this reason, the asymmetric coordinate will not contribute significantly to the width or vibronic structure of either absorption band. Therefore, only displacements along the symmetric coordinates are included in the absorption spectrum calculations. The frequencies of the symmetric modes used in the calculations were obtained from the resonance Raman spectra. The displacements were determined from the resonance Raman intensities. To fit the low-energy band, the modes that were resonantly enhanced in the Raman spectrum obtained using 676 nm excitation were used. As listed in Table 1, the symmetric mode frequencies (displacements) used to fit the low-energy band are: 827 (0.36), 864 (0.26), 1215 (0.51), 1336 (0.43), 1607 (0.59), 1635 cm^{-1} (0.24). As shown in Figure 6, with the use of these parameters the calculated spectrum is an excellent fit to the band shape of the low-energy experimental absorption spectrum.

The vibronic progression of the lower-energy band exhibits a missing mode effect (MIME).[8,67−70] While the peak spacing in this absorption band is 1395 cm^{-1}, no vibrational mode of that frequency occurs in the resonance Raman spectrum. (The frequencies in the excited electronic state in general will be different from those in the ground state and probably smaller, but the nearest likely candidate is the mode with a ground-state frequency of 1543 cm^{-1}.) The single, regularly spaced progression results from the combination of the actual frequencies listed in Table 1. This phenomenon is best illustrated in the time domain since the partial recurrence of the propagating wavepacket at time t_M is responsible for the appearance of a regularly spaced progression at a frequency $\omega = c^{-1}t_M{}^{-1}$.[8,67−70] Consider the two most highly displaced modes from Table 1 with frequencies 1215 and 1607 cm^{-1}. Treating each mode separately, (i.e., propagating the wavepacket on a harmonic surface with a frequency of either 1215 or 1607 cm^{-1}) leads to a recurrence time of 27.5 fs for the 1215 cm^{-1} mode case and 20.8 fs for the 1607 cm^{-1} mode case as indicated in Figure 7. However, when both modes are included and the damping factor is significantly large, one recurrence time is observed at 23.5 fs which corresponds to a vibrational peak spacing of 1420 cm^{-1}. The vibronic structure in the experimental spectrum in Figure 1 with 1395 cm^{-1} peak spacing was fit by using all six of the resonantly enhanced modes.

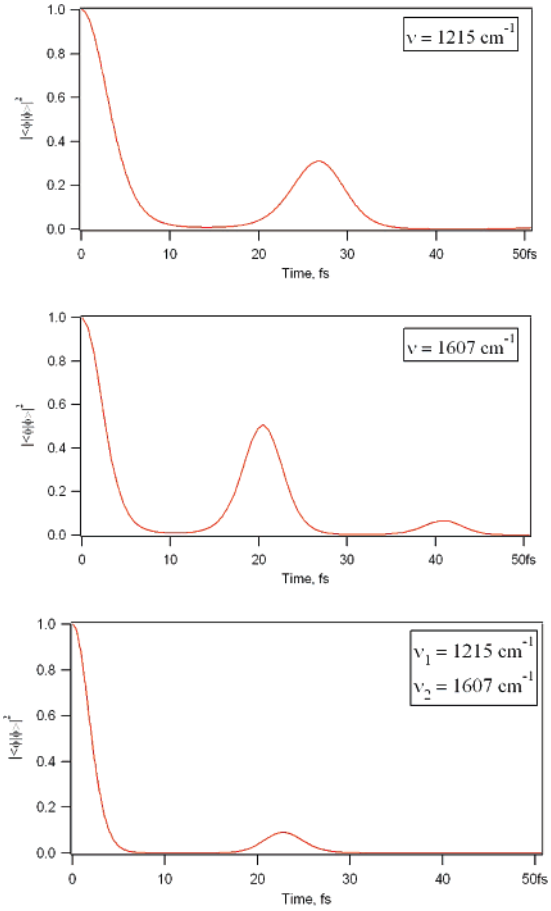

Figure 7. Time domain illustration of the MIME using a two-mode example. (Top) $|\langle\phi|\phi(t)\rangle|^2$ for $\nu_1 = 1215$ cm^{-1}. (Middle) $|\langle\phi|\phi(t)\rangle|^2$ for $\nu_2 = 1607$ cm^{-1}. (Bottom) $|\langle\phi|\phi(t)\rangle|^2$ resulting from the product of ν_1 and ν_2 overlaps.

The high-energy band was fit using the frequencies from the resonance Raman spectrum obtained with 458 nm excitation. Table 1 shows two sets of displacements for these enhanced modes: one set obtained directly from the resonance Raman intensities and the other set that was used to fit the vibronic structure of the absorption band. The deviation from the set of displacements obtained from resonance Raman intensities results from the breakdown of Savin's formula which only gives good estimates of the relative displacements of the modes when resonance Raman excitation profiles are smooth and stucture-

(67) Tutt, L.; Tannor, D.; Heller, E. J.; Zink, J. I. *Inorg. Chem.* **1982**, *21*, 3858.
(68) Tutt, L.; Tannor, D.; Schindler, J.; Heller, E. J.; Zink, J. I. *J. Phys. Chem.* **1983**, *87*, 3017.
(69) Tutt, L.; Zink, J. I. *J. Am. Chem. Soc.* **1986**, *108*, 5830.
(70) Tutt, L.; Zink, J. I.; Heller, E. J. *Inorg. Chem.* **1987**, *26*, 2158.

less.[36,38] The symmetric mode dimensionless displacements (Δ) used to fit the high-energy band were: 705 (1.05), 827 (0.45), 864 (0.3), 977 (0.2), 991 (0.3) 1215 (0.4), 1336 (0.2), 1543 (0.3) 1570 (0.1) 1607 (0.15), 1655 (0.05), 1688 (0.07), 1816 cm^{-1} (0.74). The calculated fit is shown in Figure 6.

The different appearance of the vibronic structure between the high- and low-energy absorption bands is consistent with our interpretation based on the neighboring orbital model. The electronic transition from the phenyls to the $(NN)^+$, which gives rise to the low-energy band, involves modes with significant NN and phenyl displacements, as revealed by the resonance Raman spectrum. The combination of these modes gives rise to the observed vibronic progression in the absorption spectrum. The high-energy band arises predominantly from the hydrazine π,π^* transition, that is, $E_1 \rightarrow E_4$. For this type of transition, modes that involve NN displacement are expected to be important. Both the low-frequency component of the vibronic progression of this band as well as the resonance Raman data indicates that the 705 cm^{-1} mode, which is assigned as an NN twist, is one of the most highly displaced modes. Since the hydrazine unit is coupled to the phenyl groups, vibrations involving the phenyls are also expected to be enhanced. The higher-frequency component of the vibronic structure in the absorption spectrum is therefore attributed to the phenyl CC stretching modes that are enhanced in the resonance Raman spectrum.

6. Summary

The absorption spectrum of $\mathbf{1}^+$ contains the two components, one dipole allowed and the other vibronically allowed, that are characteristic of a molecule with a mixed-valence excited electronic state and antiparallel transition dipole moments. The observed energy ordering of the two components is caused by a positive coupling in the excited state; the sign of the coupling is explained by the neighboring orbital model. The absorption spectra contain the first example of vibronic structure in a hydrazine radical cation, and apparently the first for an ESMV transition. Resonance Raman spectroscopy is used with the time-dependent theory of spectroscopy to determine the largest excited-state distortions. The normal-mode frequencies used to calculate the spectrum were obtained from resonance Raman spectroscopy, and the displacements were determined by the vibronic structure of each absorption band. Using these parameters, excellent fits to the absorption spectra were obtained. In the lowest-energy ESMV excited state that involves charge transfer from the phenyls to the hydrazine, significant NN and phenyl displacements were revealed by the resonance Raman intensities. These displacements give rise to the observed vibronic progression in the electronic absorption spectrum. The regular spacing does not correspond to a single normal mode and is an example of the missing mode effect. The high-energy band, arising from the hydrazine π,π^* transition, involves NN motions. The resonance Raman data indicate that the 705 cm^{-1} mode, which is assigned as an NN twist, is one of the most highly displaced modes and is manifested by the low-frequency component of the vibronic progression. The combination of experiment and theory provides a detailed picture of the mixed-valence excited state.

Acknowledgment. This work was made possible by grants from the National Science Foundation (CHE-0240197 to S.F.N. and CHE-0507929 to J.I.Z.).

Supporting Information Available: Complete reference 56. This material is available free of charge via the Internet at http://pubs.acs.org.

JA0609093